

Bose-Hubbard model on a star lattice

Sergei V. Isakov⁽¹⁾, K. Sengupta⁽²⁾ and Yong Baek Kim^(3,4)

⁽¹⁾ *Institute for Theoretical Physics, ETH Zürich, CH-8093 Zürich, Switzerland.*

⁽²⁾ *Theoretical Physics Division, Indian Association for the Cultivation of Sciences, Kolkata-700032, India.*

⁽³⁾ *Department of Physics, University of Toronto, Toronto, Ontario M5S 1A7, Canada.*

⁽⁴⁾ *School of Physics, Korea Institute for Advanced Study, Seoul 130-722, Korea.*

(Dated: November 2, 2018)

We analyze the Bose-Hubbard model of hardcore bosons with nearest neighbor hopping and repulsive interactions on a star lattice using both quantum Monte Carlo simulation and dual vortex theory. We obtain the phase diagram of this model as a function of the chemical potential and the relative strength of hopping and interaction. In the strong interaction regime, we find that the Mott phases of the model at $1/2$ and $1/3$ fillings, in contrast to their counterparts on square, triangular, and Kagome lattices, are either translationally invariant resonant valence bond (RVB) phases with no density-wave order or have coexisting density-wave and RVB orders. We also find that upon increasing the relative strength of hopping and interaction, the translationally invariant Mott states undergo direct second order superfluid-insulator quantum phase transitions. We compute the critical exponents for these transitions and argue using the dual vortex picture that the transitions, when approached through the tip of the Mott lobe, belong to the inverted XY universality class.

PACS numbers: 75.10.Jm, 05.30.Jp, 71.27.+a, 75.40.Mg

I. INTRODUCTION

The study of microscopic models which may lead to exotic quantum phases has been carried on for a long time in condensed matter physics. Recently, one such model system, namely, the two-dimensional (2D) Bose-Hubbard model on a lattice, has received a great deal of attention. One of the reasons for this renewed attention is the possibility of experimental realization of such a model using cold atoms trapped in optical lattices.^{1,2} However, the Bose-Hubbard model is theoretically interesting in its own right. In particular, it has recently been pointed out that the superfluid-insulator transitions for fractional Boson filling factors in this model may be of non Landau-Ginzburg type in the sense that the low energy theory for these transitions cannot be described in terms of order parameter fields of the phases in either side of the transitions.³ Instead, as pointed out in several studies of the model,^{3,4,5} the transition is aptly described in terms of vortices which are topological excitations of the superfluid and whose condensation ultimately leads to destabilization of the superfluid phase in favor of insulating Mott phases.³ Such a dual vortex theory provides a list of possible competing Mott phases via general symmetry requirements of the underlying lattice.³ In particular the geometric frustration induced by the lattice structure, which plays a key role in determining the nature of these competing Mott phases, is quite naturally described by the dual vortex theory.

Another, more direct and quantitative, approach to studying these Bose-Hubbard models on a lattice has been numerical quantum Monte Carlo (QMC) simulations.^{6,7,8} These QMC studies provide us with quantitatively accurate phase diagrams of the model. Further, they also furnish direct information about both the nature of the phase transition and the correlation

functions in the Mott phase.^{6,8,9} These features, along with the possibility of accessing much larger system sizes than possible in exact diagonalization studies, make them the numerical method of choice for the lattice Bose-Hubbard models. A combination of the dual vortex theory and QMC simulation has been recently used to study the phases of Bose Hubbard model on triangular^{4,8} and Kagome lattices.^{5,6} As noted in these works, the Bose-Hubbard model can also be mapped onto a spin-1/2 XXZ model⁵ leading to interpretation of the obtained results in terms of both bosons and quantum spins.

More recently, there have been several studies of the antiferromagnetic Heisenberg model on a star lattice.^{10,11,12} This lattice, shown in Fig. 1, can be constructed by expanding the sites of a hexagonal lattice into triangles. It consists of two topologically inequivalent bonds, triangular and expanded, as shown in Fig. 1. It has been argued in Ref. 11, using exact diagonalization studies, that the ground state of the Heisenberg model on this lattice is a paramagnetic valence bond crystal (VBC). Such a VBC state is characterized by enhanced antiferromagnetic correlations along the expanded bonds indicating singlet formation along those bonds. Such studies have also been extended for the anisotropic antiferromagnetic Heisenberg model where the exchange coupling J^T on triangles is different from the coupling J^E on expanded links.¹⁰ It has been argued in Ref. 10 that there may be another VBC state for $J^T \gtrsim 1.3J^E$ which consists of 18-site star pattern. Possible spin liquid and valence bond crystal phases are also studied in an $Sp(N)$ generalized model.¹³ These studies, till date, have not been extended to other spin models such as the XXZ model.

In this work, we study the Bose-Hubbard model, or equivalently, the XXZ model on a star lattice. The Hamiltonian of the model can be represented in terms

of hardcore bosons as

$$H_b = - \sum_{\langle ij \rangle} \left(t^{ij} b_i^\dagger b_j + \text{h.c.} \right) + \sum_{\langle ij \rangle} V^{ij} n_i n_j - \mu \sum_i n_i \quad (1)$$

where $t^{ij}(V^{ij})$ is the hopping amplitude (interaction strength) of the Bosons between sites i and j , b_i denotes annihilation operator of the boson at site i , $n_i = b_i^\dagger b_i$ is the number density operator for the Bosons at site i , $\langle ij \rangle$ indicates that sites i and j are nearest neighbors of each other, and μ is the chemical potential. This model, in contrast to the Heisenberg model on frustrated lattices, is amenable to QMC studies. In what follows, we shall allow for different amplitudes of hopping amplitude and interaction strengths: $t^{ij} = t^E$ and $V^{ij} = V^E$ for expanded bonds and $t^{ij} = t^T$ and $V^{ij} = V^T$ for triangular bonds. In this work, we shall set $t^E/t^T = V^E/V^T$. We note at the outset that this model can be mapped onto an XXZ model in a magnetic field via a Holstein-Primakoff transformation⁵ and yields

$$H_{\text{XXZ}} = -\frac{1}{2} \sum_{\langle ij \rangle} J_{\perp}^{ij} [S_i^+ S_j^- + S_i^- S_j^+] + \sum_{\langle ij \rangle} J_z^{ij} S_i^z S_j^z + h_z \sum_i S_i^z, \quad (2)$$

where $J_{\perp}^{ij} = t^{ij}$, $J_z^{ij} = V^{ij}$, $h_z = (\mu - 1/2)$, and the spin operators are expressed in terms of the boson operators as $S_i^+ = b_i^\dagger$, $S_i^- = b_i$, $S_i^z = b_i^\dagger b_i - 1/2$ in the leading order in $1/S$. We shall use these spin and the boson representations of the model interchangeably throughout the paper. Note that half filling in boson language means zero magnetic field in spin language.

The central results reported in this work are the following. First, using QMC simulation for sufficiently large systems ($L \leq 60$) and low temperatures ($\beta^{-1} \leq 0.001 J_{\perp}$), we obtain a phase diagram of the Bose-Hubbard (XXZ) model as a function of the μ/V^E (h_z/J_z^E) and t^E/V^E (J_{\perp}^E/J_z^E) for fixed ratios V^T/V^E (t^T/t^E). We find that there are three distinct Mott phases at boson fillings $1/2$ and $1/3$. Second, using QMC simulations, we compute the equal-time spin-spin correlation functions and the real space bond-bond correlation functions for the bosons (spins). From these studies, we demonstrate that two of these Mott phases, which occur for $J^T = J^E$ at $1/2$ and $1/3$ fillings, are translationally invariant and do not exhibit density-wave order (magnetization). These Mott states, in stark contrast to their counterparts in square, triangular or Kagome lattices,^{7,8,9} are found to have resonating valence bonds (RVB) along either the triangle or the expanded links. The third Mott phase has coexisting density-wave (Néel) and RVB orders and occur for $J^T \neq J^E$ and at $1/2$ filling. These QMC results regarding the nature of the Mott phases are also supported by qualitative symmetry-based analysis using dual vortex theory. Third, the translationally invariant Mott states occurring for $J^T = J^E$ are

found to undergo a second-order superfluid-Mott insulator quantum phase transition with increasing t^E/V^E (in the spin language, this transition corresponds to a shift from S_x to S_z ordering if S_z ordering is present or from S_x ordering to a paramagnet if such an ordering is absent). This is also in contrast to analogous studies on square, triangular and Kagome lattices,^{7,8,9} where QMC simulations found evidence of either a direct first-order transition between the superfluid and the Mott phases or an intermediate supersolid phase. A qualitative symmetry-based analysis using the dual vortex theory finds this transition to be in the inverted XY universality class, when the transition point is approached through the tip of the Mott lobes. This observation is also supported by a finite-size scaling studies using QMC simulations which yields the dynamical critical exponent z and the correlation length exponent ν for the transition.

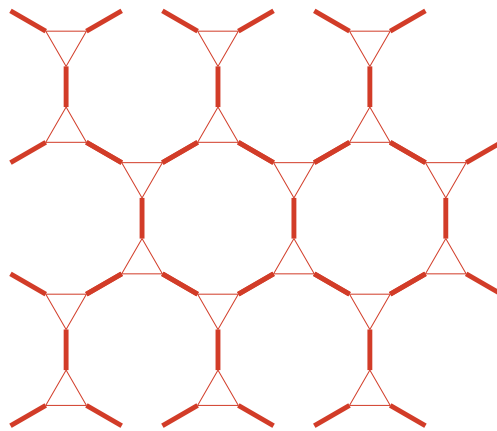


FIG. 1: The star lattice. The 'triangle' bonds are denoted by thin lines and the 'expanded' bonds are denoted by thick lines.

The organization for the rest of this work is as follows. In Sec. II, we elucidate our QMC results. We deal with the case $J_{\perp}^T = J_{\perp}^E$ in Sec. IIA and follow it up with the study of the case $J_{\perp}^T \neq J_{\perp}^E$ for $1/2$ filling in Sec. IIB. These numerical results are then compared with the analytical predictions of the dual vortex theory in Sec. III. This is followed by conclusion in Sec. IV.

II. QUANTUM MONTE CARLO

In this section, we shall analyze the model using quantum Monte Carlo. We use a multi-site generalization¹⁴ of the stochastic series expansion (SSE) method.¹⁵ Here the basic lattice unit is a site and all its neighbors. Simulations are performed for systems of linear size $L = 12, 18, 24, 36, 48, 60$ with $N = 6L^2$ sites at different temperatures (the lowest temperature is $\beta^{-1} = J_{\perp}/1200$). In Sec. IIA, we study the isotropic case with equal hopping and interaction strength on the triangle and expanded bonds while the anisotropic case is studied in Sec. IIB.

A. $J^T = J^E$

1. Phase diagram

The phase diagram obtained for $J^T = J^E$ is shown in Fig. 2. There are three phases: the XY ferromagnet and two valence bond crystals denoted by VBC1 and VBC2. In the boson language, they correspond to the superfluid and Mott phases respectively. The characteristics of these Mott phases and their transition to the superfluid phase is discussed in Sec II A 2 and II A 3 in details. We note here that the Monte Carlo scans are performed only along three lines shown in the phase diagram so that the phase boundaries are approximate.

2. Half filling

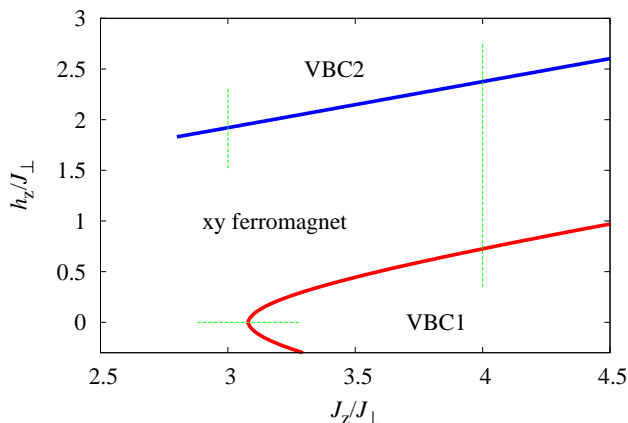


FIG. 2: The schematic $J^T = J^E$ phase diagram from Monte Carlo simulations. The phase boundaries are denoted by thick solid lines. Monte Carlo scans are denoted by dashed lines.

In this subsection, we focus on the model in the absence of an applied magnetic field, *i.e.* at 1/2 filling for bosons. There is a continuous transition from the superfluid phase to an insulating phase at $J_z/J_\perp \approx 3.0783$. In the vicinity of a continuous transition, the spin-stiffness of the XY ferromagnet (or superfluid density in the boson language), ρ_s , which is measured through winding number fluctuations, scales as

$$\rho_s = L^{-z} F_{\rho_s}(L^{1/\nu}(K_c - K), \beta/L^z), \quad (3)$$

where F_{ρ_s} is the scaling function, L is the linear system size, z is the dynamical critical exponent, ν is the correlation length exponent, $\delta K_c = K_c - K = (J_z/J_\perp)_c - J_z/J_\perp$ is the distance to the critical point, $\beta = (k_B T)^{-1}$ is the inverse temperature, and k_B is the Boltzmann constant. It follows from the above finite size scaling relation (Eq. 3) that the curves for different systems sizes should cross

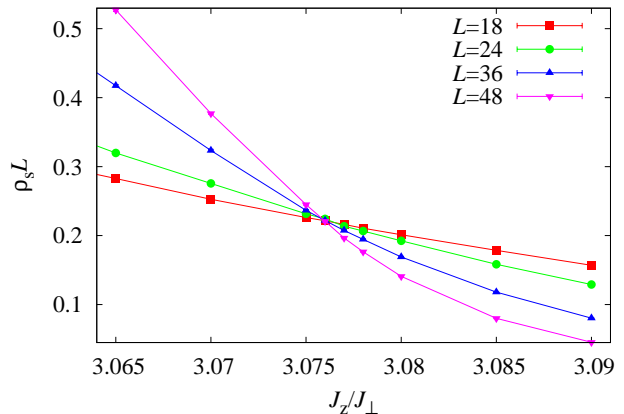


FIG. 3: Scaling of the superfluid density ρ_s for $z = 1$, $\beta = 16L/J_\perp$ and $h_z/J_\perp = 0$. Lines guide the eye. In this and all other figures, error bars are smaller than the symbol size if not visible.

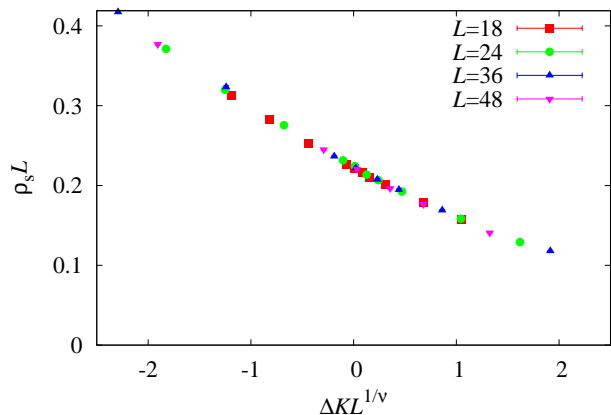


FIG. 4: Data collapse of the superfluid density ρ_s for $z = 1$, $\nu = 0.67$, $(J_z/J_\perp)_c = 3.0783$, $\beta = 16L/J_\perp$, and $h_z/J_\perp = 0$.

at the transition point when $\rho_s L^z$ is plotted as a function of the coupling constant for β/L^z fixed (or for large enough β to ensure the ground state convergence). It also follows from Eq. 3 that the curves for different system sizes should collapse onto a universal curve for appropriate values of ν and $(J_z/J_\perp)_c$ when $\rho_s L^z$ is plotted as a function of $\delta K_c L^{1/\nu}$. The data scale well with the dynamical critical exponent $z = 1$. In Fig. 3, $\rho_s L$ is shown as a function of the coupling constant. The curves for different system sizes cross at a distinct point. The data collapse is shown in Fig. 4 and leads to a critical exponent $\nu = 0.67$.

To address the nature of the insulating phase for $J_z \gg J_\perp$, we study the equal time and static spin structure factors that are given by

$$S(\mathbf{q}) = L^2 \langle S_{\mathbf{q}\tau}^\dagger S_{\mathbf{q}\tau} \rangle, \quad \chi(\mathbf{q}) = L^2 \left\langle \int d\tau S_{\mathbf{q}\tau}^\dagger S_{\mathbf{q}0} \right\rangle \quad (4)$$

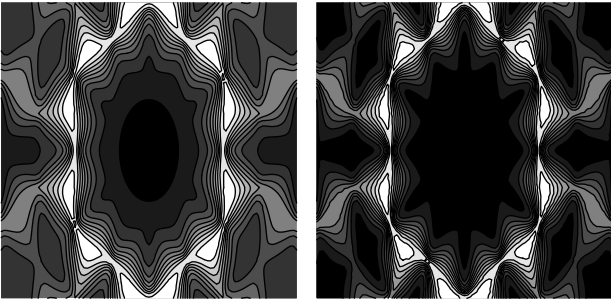


FIG. 5: The equal time spin-spin structure factor (left panel) and the static structure factor (right panel) for $L = 24$, $J_z/J_\perp = 4$, $h_z/J_\perp = 0$, and $k_B T = 0.002 J_\perp$. The axes range from -4π to 4π .

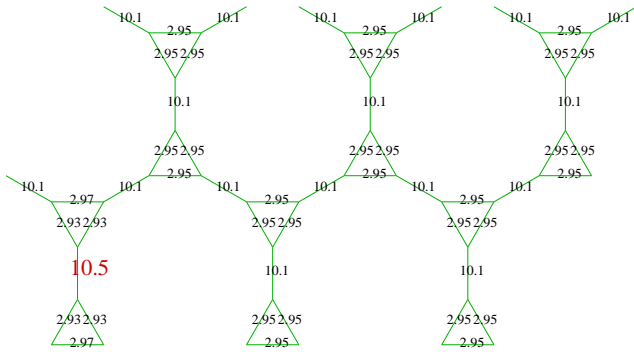


FIG. 6: The correlation function $C_b(\mathbf{r}_1 - \mathbf{r}_\delta)$ between the bond indicated by a large text and the other bonds for $L = 24$, $J_z/J_\perp = 4$, $h_z/J_\perp = 0$, and $k_B T = 0.01 J_\perp$.

where $S_{\mathbf{q}\tau} = (1/L^2) \sum_i S_{i\tau}^z \exp(i\mathbf{q} \cdot \mathbf{r}_i)$. The structure factors in the insulating phase are shown in Fig. 5. There are no sharp peaks which is a clear indication of absence of magnetic order. The short-range bow-tie features, found to be present in the structure factor, are likely to be a remnant of classical dipolar correlations at finite temperatures, that are known to arise in classical Heisenberg models on various frustrated lattice.

The nearest neighbor antiferromagnetic spin-spin correlations are strongly enhanced along the expanded bonds (bonds that connect triangles) signaling singlet formation along those bonds: $\langle [S^z S^z]_e \rangle \approx 2.92 \langle [S^z S^z]_t \rangle$ for $J_z/J_\perp = 4$, $h_z/J_\perp = 0$, and $T = 0.01 J_\perp$. To verify this, we further compute the real space bond-bond correlation function that is given by

$$C_b(\mathbf{r}_\gamma - \mathbf{r}_\delta) = \left\langle \frac{1}{\beta} \int B_{\gamma\tau} d\tau \int B_{\delta\tau} d\tau \right\rangle, \quad (5)$$

where $B_{\alpha(i,j),\tau} = J_\perp (S_i^x S_j^x + S_i^y S_j^y)$ is the off-diagonal bond operator (at imaginary time τ) of the bond α connecting spins i and j . A plot of $C_b(\mathbf{r}_\gamma - \mathbf{r}_\delta)$ in Fig. 6 shows that the off-diagonal bond operators are distributed uniformly on the expanded and triangle bonds with the majority of operators on the expanded bonds with a ratio $10.1/2.95 \approx 3.42$. There is no any other bond order.

Thus the real-space bond-bond correlation function also confirms the formation of singlets along the expanded bonds. This lead us to conclude that the most probable candidate for this insulating phase is VBC with no symmetry breaking and is analogous to the VBC state described in Ref. 11. We denote this phase as VBC1.

3. $1/3$ filling

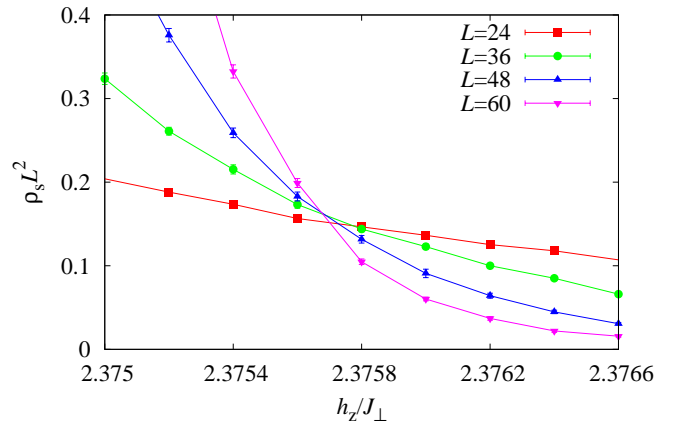


FIG. 7: Scaling of the superfluid density ρ_s for $z = 2$, $\beta = L^2/3 J_\perp$, and $J_z/J_\perp = 4$. Lines guide the eye.

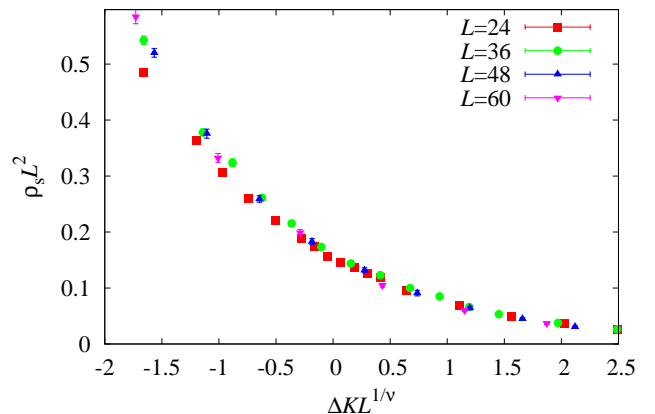


FIG. 8: Data collapse of the superfluid density ρ_s for $z = 2$, $\nu = 0.5$, $(h_z/J_\perp)_c = 2.37568$, $\beta = L^2/3 J_\perp$. $\Delta K = (h_z/J_\perp)_c - h_z/J_\perp$ at fixed $J_z/J_\perp = 4$.

In this subsection, we focus on the phase diagram away from the $1/2$ filling, or, in the spin language, in the presence of an applied longitudinal magnetic field. As shown in Fig. 2, there is an additional VBC phase (denoted as VBC2) at the filling of $1/3$ (spin magnetization equals $-1/6$). The transition from the XY ferromagnet phase to the VBC2 phase is continuous. Within the system

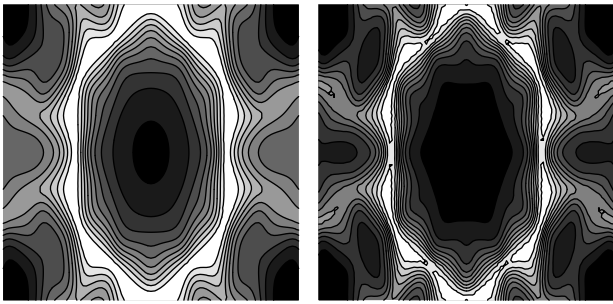


FIG. 9: The equal time spin-spin structure factor (left panel) and the static structure factor (right panel) for $L = 24$, $J_z/J_\perp = 4$, $h_z/J_\perp = 3$ and $k_B T = 0.005 J_\perp$. Ferromagnetic peaks due to the uniform background magnetization are subtracted. The axes range from -4π to 4π .

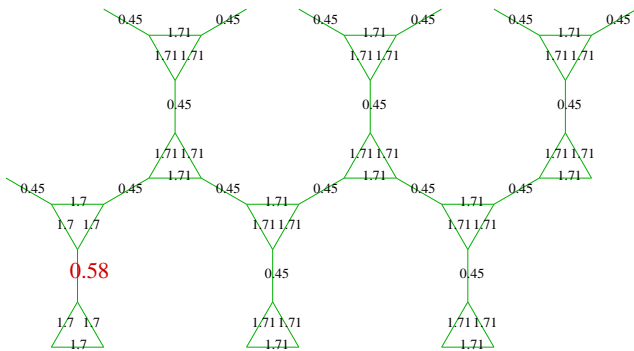


FIG. 10: The correlation function $C_b(\mathbf{r}_1 - \mathbf{r}_\delta)$ between the bond indicated by a large text and the other bonds for $L = 24$, $J_z/J_\perp = 4$, $h_z/J_\perp = 3$, and $k_B T = 0.01 J_\perp$.

size and temperatures that we have studied, we have not found any signatures of a first order transition such as double peaked histograms. As shown in Fig. 7 and Fig. 8, the data scale reasonably well with $z = 2$ and $\nu = 0.5$. It is worth mentioning that the scaling is not as good as that for the transition to the VBC1 phase described in the previous section. The quality of the scaling is probably limited by the fact one needs data of very high accuracy at extremely low temperatures and very large system sizes (in order to reach the scaling regime given by Eq. 3) and that is beyond our computational facilities at the present time.

As shown in Fig. 9, the VBC2 phase does not exhibit magnetic order. The connected spin correlation function is shorter-ranged than the spin correlation function in the VBC1 phase. This can be deduced from the larger bow tie width in Fig. 9 compared to Fig. 5. The nearest neighbor antiferromagnetic spin-spin correlations are slightly weaker along the expanded bonds: $\langle [S^z S^z]_e \rangle \approx 0.78 \langle [S^z S^z]_t \rangle$ for $J_z/J_\perp = 4$, $h_z/J_\perp = 3$, and $k_B T = 0.01 J_\perp$. As shown in Fig. 10, the ratio of the number of the off-diagonal operators on the expanded bonds to that on the triangle bonds is $0.45/1.71 \approx 0.26$. Thus, in contrast to the VBC1 phase, the spins resonate along

the triangle bonds in the VBC2 phase forming trimers. There is no other bond order. We can conclude that the VBC2 phase is a quantum paramagnetic phase without any symmetry breaking.

B. $J^T \neq J^E$ at $h_z = 0$

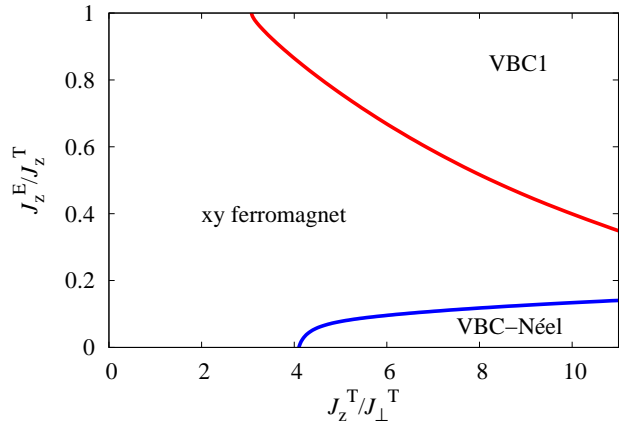


FIG. 11: The schematic $J^T \neq J^E$ phase diagram at $1/2$ filling from Monte Carlo simulations. The phase boundaries are denoted by thick solid lines.

The schematic $J^T \neq J^E$ phase diagram at $1/2$ filling is shown in Fig. 11. There are again three phases: the XY ferromagnet (superfluid in the boson language), the valence bond crystal phase from Sec. II A (VBC1), and a phase that is characterized by both VBC order and Néel-like magnetic order and is denoted as VBC-Néel. The latter two phases are Mott states in the boson language. Monte Carlo scans are performed only along a few lines so that the phase boundaries are approximate. We have not attempted to determine the nature of phase transitions. However, as shown in Fig. 12, we find a narrow region with finite superfluid density between the VBC1 and VBC-Néel phases even for large J_z^T/J_\perp^T .

In Fig. 13, we show the real space bond-bond correlation function for different values of J_z^E/J_z^T . There are singlets on the expanded bonds for large J_z^E/J_z^T (VBC1 phase) and there are resonating triangles (trimers) for small J_z^E/J_z^T (VBC-Néel phase). The VBC-Néel phase also exhibits long range magnetic order. In Fig. 14, we show the finite size scaling of the equal time structure factor given by Eq. 4 at the ordering wave vector $\mathbf{Q} = (2\pi, 2\pi)$. Note that the structure factor vanishes at $\mathbf{Q} = (0, 0)$ due to geometrical factors. The structure factor divided by the number of lattice sites clearly scales to a finite value in the thermodynamic limit indicating long-ranged magnetic order. The triangles of the star lattice form the bipartite hexagonal lattice. The structure of the real space correlations is such that the spins on two different sublattices of the hexagonal lattice (belonging

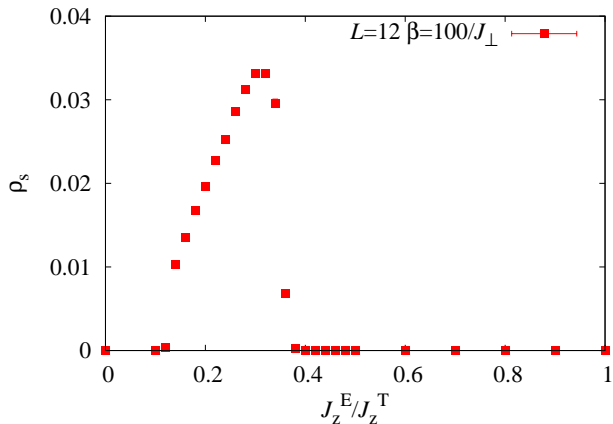


FIG. 12: The superfluid density ρ_s as a function of J_z^E/J_z^T for $J_z^T/J_\perp^T = 10$, $L = 12$, and $k_B T = 0.01 J_\perp^T$.

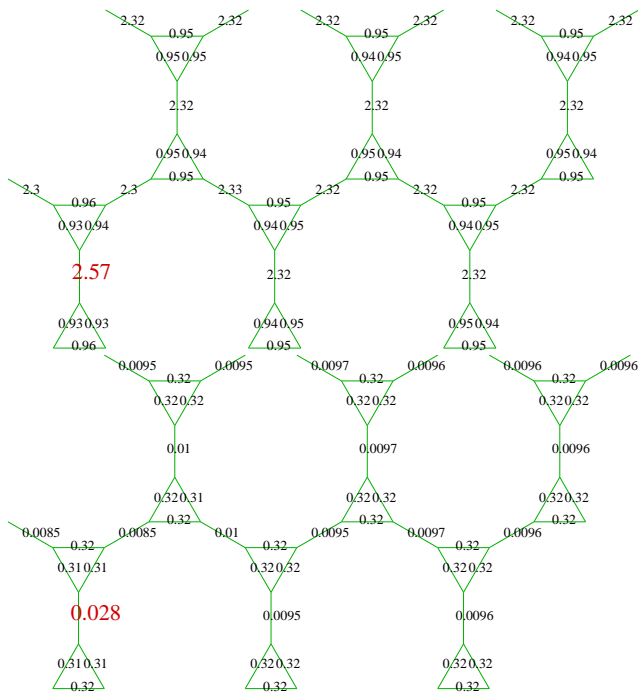


FIG. 13: The correlation function $C_b(\mathbf{r}_1 - \mathbf{r}_s)$ between the bond indicated by a large text and the other bonds in the VBC1 phase at $J_z^E/J_z^T = 0.6$ (upper panel) and in the VBC-Néel phase at $J_z^E/J_z^T = 0.1$ (lower panel) for $J_z^T/J_\perp^T = 10$, $L = 12$, and $k_B T = 0.01 J_\perp^T$.

to up and down triangles in Fig. 1) have antiferromagnetic correlations as in a Néel-like ordered state. This long-ranged magnetic order corresponds to density-wave order in the boson language.

To understand the VBC-Néel state in more detail, consider isolated triangles ($J^E = 0$). There are two degenerate ground states per triangle. These are resonating

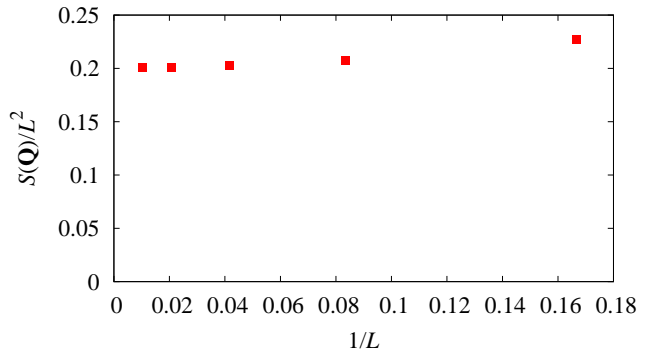


FIG. 14: The equal time structure factor at the ordering wave vector \mathbf{Q} as a function of the inverse system size for $J_z^T/J_\perp^T = 10$, $L = 12$, and $k_B T = 0.01 J_\perp^T$.

trimers with the total spin $S^z = -1/2$

$$|\psi_1\rangle = \frac{1}{\sqrt{3}}(|--+) + |-+-\rangle + |+-\rangle)$$

and the total spin $S^z = 1/2$

$$|\psi_2\rangle = \frac{1}{\sqrt{3}}(|++-\rangle + |+-+\rangle + |-++\rangle),$$

where $+$ ($-$) indicate sites with $S^z = 1/2$ ($-1/2$). In the boson language, $|\psi_1\rangle$ and $|\psi_2\rangle$ correspond to one and two bosons per triangle respectively. At $1/2$ filling, the number of spin up triangles is equal to the number of spin down triangles. For $J^E = 0$, those triangles can be arranged arbitrary on the star lattice and the ground state is extensively degenerate. However, finite J^E selects a Néel state with respect to the total spins of the triangles because the triangles form a bipartite lattice and the effective interaction between them is antiferromagnetic. A similar state is also found in the dual vortex theory analysis, see the next section.

III. DUAL VORTEX THEORY

In this section, we shall obtain an analytical understanding of the nature of the Mott phase and the quantum phase transitions from them to the superfluid phases. Throughout this section, we shall restrict ourselves to the isotropic case $J^T = J^E$.

The derivation of a dual vortex action starting from the Bose-Hubbard model (Eq. 1) has been elaborated in Refs. 3,4,5. The vortices are described in terms bosonic field ψ_b and a dual gauge field $A_{b\mu}$ which lives on the sites b and links μ of the dual lattice respectively. A duality analysis of the Bose-Hubbard model then leads to an effective dual action which can be expressed in terms

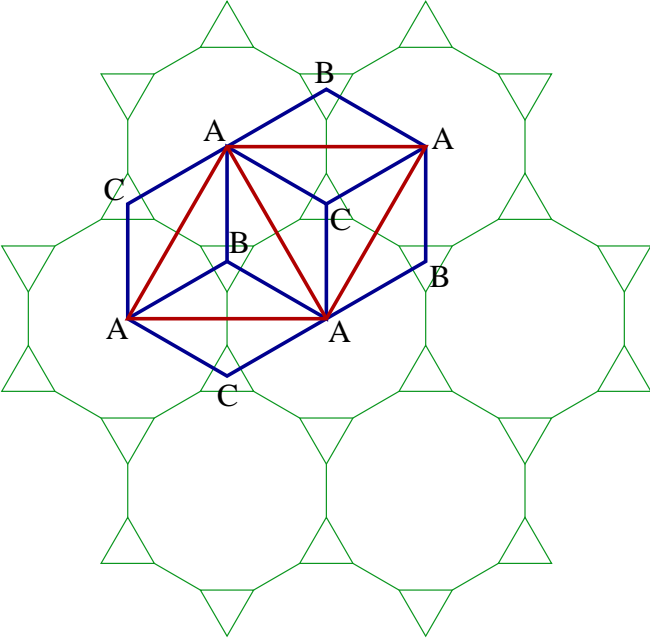


FIG. 15: The star lattice and its dual. Notice that the A sites are in the center of the hexagon of the dual lattice while the B and the C sites are in the center of the triangle.

of the vortices and the gauge fields as³

$$\begin{aligned}
Z &= \int \mathcal{D}A \int \mathcal{D}\theta \exp(-S_d) \\
S_d &= \frac{1}{2e^2} \sum_b (\epsilon_{\mu\nu\lambda} \Delta_\nu A_{b\lambda} - f \delta_{\mu\tau})^2 \\
&\quad - y_v \sum_b (\psi_{b+\mu} e^{2\pi i A_{b\mu}} \psi_b + \text{h.c.}) \\
&\quad + \sum_b \left(r |\psi_b|^2 + u |\psi_b|^4 \right) \quad (6)
\end{aligned}$$

where ψ_b are the vortex field living on the site b of the dual lattice, $A_{b\mu}$ is the U(1) dual gauge field such that $\epsilon_{\tau\nu\lambda} \Delta_\nu A_{b\lambda} = n_i$ where n_i is the physical boson density at site i , \sum_p denotes sum over elementary plaquette of the dual lattice, Δ_μ denotes lattice derivative along $\mu = x, y, \tau$, and f is the average boson density. Here y_v is the vortex fugacity and r , u , and e denotes parameters of the dual action which can not be directly mapped onto those of H_b since S_d is not self-dual to the boson action obtained from H_b . Therefore we cannot, in general, obtain a direct mapping between the parameters of the two actions, except for identifying the magnetic field seen by the vortices $\epsilon_{\tau\nu\lambda} \Delta_\nu A_{b\lambda}$ as the physical boson density.^{3,4,5} In the remainder of the paper, we shall classify the phases of this action based on symmetry consideration and within the saddle point approximation where the gauge fields are pinned to their saddle point values.

The star-lattice and its dual is shown in Fig. 15. The first step towards understanding the phases of S_d within a

saddle point approximation amounts to solving the Hopfstadter problem for the vortices on this dual lattice shown in Fig. 15. We note from Fig. 15 that the lattice dual to the star represents a dice lattice with all diagonals connecting the A sites joined to each other. The Hamiltonian of the vortices on such a lattice is given by

$$H = -y_v \sum_{\langle ij \rangle} \sum_{\alpha, \beta = A, B, C} \left(\psi_{i\alpha}^\dagger \psi_{j\beta} e^{i\gamma_{ij}} + \text{h.c.} \right) \quad (7)$$

where $\psi_{i\alpha} \equiv \psi_\alpha(a_x, a_y)$ denotes the annihilation operator for vortex fields at $i \equiv (a_x, a_y)$ and γ_{ij} is the dual magnetic flux, which in the gauge $\vec{A} = H(0, x)$, is given by

$$\gamma_{ij} = 2\pi f(2a_x/a + \lambda_\alpha)(y'_j - y'_i) \quad (8)$$

where we have used $x_i = a_x$, $x_j = a_x + \lambda_\alpha a$, $y' = 2y/(\sqrt{3}a)$, $f = H\sqrt{3}a^2/4\phi_0$ is the flux passing through an elementary triangle in units of basic flux quanta ϕ_0 , and λ_α is a number that depends on the sublattice index $\alpha = A, B, C$. Here the dual flux passing through an elementary plaquette is double of that of the dice lattice. This can be inferred from the fact the present lattice has two sites of the star lattice in each rhombus (as opposed to one site of the Kagome lattice in each rhombus) of the dice lattice.^{5,16}

The Schrodinger equation for the vortex fields can be constructed from the Hamiltonian. With our choice of the gauge, we can write $\psi_\alpha(a_x, a_y) = e^{i\kappa_y y'} \psi_\alpha(a_x)$, where $\kappa_y = 2ak_y/\sqrt{3} \in (0, \pi)$ since we are restricted within the first Brillouin Zone, and $\alpha = A, B, C$ represents the inequivalent sites of the dual lattice. We thus obtain, writing energy ϵ in units of t and defining $\phi_\pm = 2\pi f(2a_x/a \pm 1/2) + \kappa_y$,

$$\begin{aligned}
-\epsilon \psi_B(a_x) &= \psi_A(a_x + a) + 2\psi_A(a_x - a/2) \cos \phi_+ \quad (9) \\
-\epsilon \psi_C(a_x) &= \psi_A(a_x - a) + 2\psi_A(a_x + a/2) \cos \phi_- \quad (10) \\
-\epsilon \psi_A(a_x) &= \psi_B(a_x + a) + \psi_C(a_x - a) \\
&\quad + 2\psi_B(a_x - a/2) \cos(\phi_-) \\
&\quad + 2\psi_C(a_x + a/2) \cos(\phi_+) \\
&\quad + 2\psi_A(a_x + 3a/2) \cos(2\pi f + \phi_+) \\
&\quad + 2\psi_A(a_x - 3a/2) \cos(-2\pi f + \phi_-) \\
&\quad + 2\psi_A(a_x) \cos(\phi_+ + \phi_-) \quad (11)
\end{aligned}$$

Note that if we ignore the last three terms in the RHS of Eq. 11 which involves ψ_A , we get back the dual Hopfstadter equation for the dice lattice.^{5,16} To solve for ϵ , we substitute Eqs. 9 and 10 in Eq. 11 and get, using $a_x = 3ma/2$ for all A sites,

$$\begin{aligned}
(\epsilon^2 - 6)\psi_{Am} &= (4 \cos(2\pi f) - 2\epsilon)C_m \\
C_m &= \psi_{Am+1} \cos(6\pi f(m+1/2) + \kappa_y) \\
&\quad + \psi_{Am-1} \cos(6\pi f(m-1/2) + \kappa_y) \\
&\quad + \psi_{Am} \cos(12\pi f m + 2\kappa_y) \quad (12)
\end{aligned}$$

We first consider the case $f = 2/3$, which is identical to

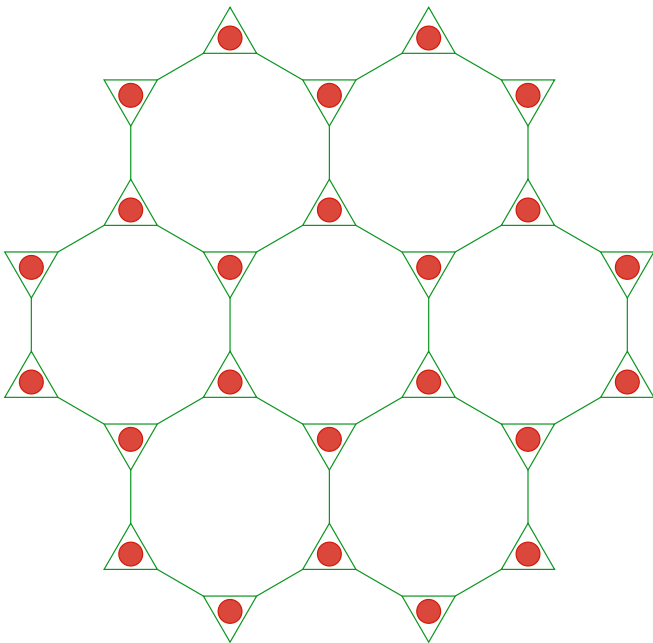


FIG. 16: Mott state at $f = 2/3$. The circles indicate a triangle with either two spin up and one spin down on the three vertices or a trimerized triangles indicated by circles when superposition of the spins/bosons due to quantum fluctuations are allowed. The state is translationally invariant and agrees with the VBC2 state predicted by QMC when quantum fluctuations are included. The corresponding ground state for $f = 1/3$ can be obtained by simply flipping the spins.

the $f = 1/3$ filling considered in Sec. II A 3. Here Eq. 12 reduces to

$$(\epsilon^2 - 6)\psi_{A\mathbf{k}} = -2(1 + \epsilon)A_{\mathbf{k}}\psi_{A\mathbf{k}} \\ A_{\mathbf{k}} = 2 \cos(k'_x) \cos(\kappa_y) + \cos(2\kappa_y) \quad (13)$$

where we have taken Fourier transform with respect to m and $k'_x = 3k_x a/2 \in (0, \pi)$. This has the solution

$$\epsilon_{\pm} = -A_{\mathbf{k}} \pm \left[(A_{\mathbf{k}} - 1)^2 + 5 \right]^{1/2} \quad (14)$$

so that the minima of the vortex spectrum occurs at $(k'_x, \kappa_y) = (0, 0), (\pi, \pi)$ and corresponds to $\epsilon = -6$. Also, substituting the values of k'_x and κ_y in Eqs. 9 and 10, we find that $\psi_B(k'_x) = 0 = \psi_C(k'_x)$ so that the eigenfunctions corresponding to $(k'_x, \kappa_y) = (0, 0), (\pi, \pi)$ are given by

$$\psi_1(m, n) = (1, 0, 0) \quad \psi_2(m, n) = (1, 0, 0)e^{i\pi(m+n)} \quad (15)$$

where we have used $a_y = \sqrt{3}na/2$ for the A sites. Note that since $m + n$ is always even for A sites $\psi_1 = \psi_2$ and hence the theory has a single vortex field which should mediate the transition. Also note that the Mott state is expected to be uniform since Ψ_1 is basically a constant. Thus the simplest state compatible with these requirement at $2/3$ filling is shown in Fig. 16. Here each triangle denoted by a circle, within mean-field, has two occupied and one empty sites leading to a net occupancy of 2

bosons per triangle. Equivalently, in the spin language, this corresponds to two spin-up and one spin-down sites at every triangle leading to a net magnetization of $1/2$. However, it is indeed possible that inclusion of quantum fluctuations will make the bonds within the triangle to resonate leading to the trimerized VBC2 state obtained in QMC studies.

The theory of transition pertains to a single vortex field in the presence of a fluctuating dual gauge field and is thus belongs to the inverted XY universality class which has $z = 1$ and $\nu = 2/3$.¹⁷ These exponents are the same as their counterparts for models in the 3D XY universality class. However, the key difference is that this exponent is obtained for a fully interacting model in $D = 2 + 1$ in the strong interacting regime. This is in contrast to $D = 3 + 1$ dimensional systems where one expects the transition to be fluctuation-driven first order.¹⁸ We note that this expectation, which was initially derived using an $\epsilon = 4 - d$ expansion method, is not valid for $D = 2 + 1$ quantum systems where such transitions remain continuous.¹⁷ Note that the quantum phase transition described by this dual vortex theory requires a fixed density across the transition and hence is valid when the transition is approached via the tip of the Mott lobe. The QMC study of Sec. II A 3 approaches the transition from the side of the lobe and hence gets a different z .

Next we come to case of $f = 1/2$. Substituting $f = 1/2$, in Eq. 12, one gets

$$(\epsilon^2 - 6)\psi_{Am} = -4(1 + \epsilon/2)C_m \\ C_m = -\psi_{Am+1} \sin(3\pi m + \kappa_y) \\ + \psi_{Am-1} \sin(3\pi m + \kappa_y) \\ + \psi_{Am} \cos(2\kappa_y) \quad (16)$$

Thus here we need to distinguish between the sites which have m as even and odd integers. Denoting the corresponding fields as ψ^e and ψ^o respectively, we find that

$$[\epsilon^2 - 6 + 4(1 + \epsilon/2) \cos(2\kappa_y)] \psi_{A\mathbf{k}}^e + C_{\mathbf{k}} \psi_{A\mathbf{k}}^o = 0 \\ [\epsilon^2 - 6 + 4(1 + \epsilon/2) \cos(2\kappa_y)] \psi_{A\mathbf{k}}^o + C_{\mathbf{k}}^* \psi_{A\mathbf{k}}^e = 0 \\ C_{\mathbf{k}} = 8i \sin(k'_x) \sin(\kappa_y)(1 + \epsilon/2) \quad (17)$$

Note that here $k'_x, \kappa_y \in (0, \pi/2)$ since the periodicity in real space has been doubled. From Eq. 17, we find that $\epsilon = -A_{\mathbf{k}\pm} \pm \sqrt{(A_{\mathbf{k}\pm} - 2)^2 + 2}$ where

$$A_{\mathbf{k}\pm} = \cos(2\kappa_y) \pm 2|\sin(k'_x)| |\sin(\kappa_y)| \quad (18)$$

Thus the minima of the spectrum occurs at $(k'_x, \kappa_y) = (\pi/2, \pi/6)$ with $\epsilon = -3$. Substituting the value of ϵ in Eq. 17, we find $\psi_A^e = i\psi_A^o$. Also, substituting the values of $\psi_A^e/\psi_A^o = i$, $k'_x = \pi/2$ and $\kappa_y = \pi/6$, we find ψ_B and ψ_C from Eq. 16. Finally, this yields the wavefunction

$$\psi_1^{e(o)} = [1(-i), 0, c(-ci)] e^{i\pi a_1} e^{i\pi a_2/6} \quad (19)$$

where $c = 2/3$, the coordinates of odd and even sites are taken to be $(a_1, a_2) = (2m + 1, 2n + 1)$ and $(a_1, a_2) =$

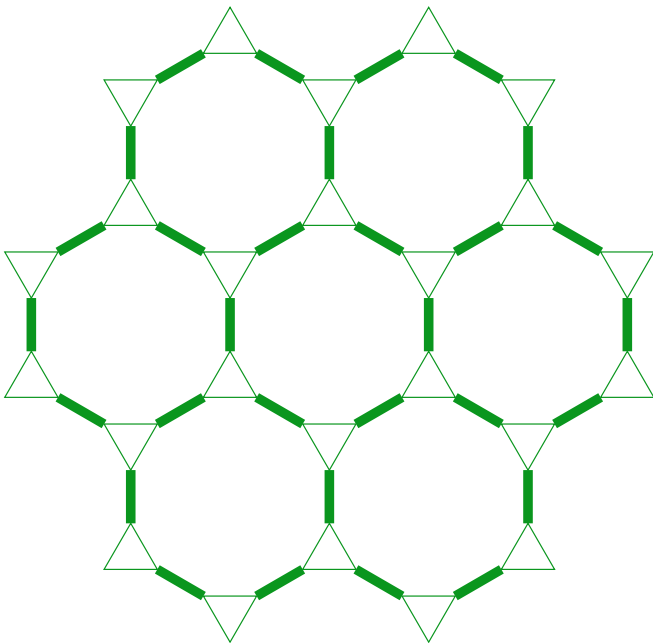


FIG. 17: A possible Mott state with all the connecting bonds of the triangles forming dimers. The dimerized bonds are shown by thick lines. This state can occur for $n = 0, 1, 2$ or 3 and is identical to the VBC1 phase predicted by QMC when quantum fluctuations are included. See text for details.

$(2m, 2n)$ and we haven't renormalized the wavefunction. Thus, the theory of transition again pertains to a theory of single vortex field in the presence of fluctuating dual gauge field and belongs to the inverted XY universality class with $z = 1$ and $\nu = 2/3$. This is compatible with the exponents obtained by QMC study in Sec. II A 2.

Finally, we consider the possible Mott states for $f = 1/2$. These are obtained from qualitative argument outlined below and are shown in Figs. 17, and 18. From the vortex wave function (Eq. 19), we find that all the B sites of the dual lattice are equivalent. Thus the triangles of the star lattice whose centers are occupied by B sites of the dual lattice must have the same filling and can be filled with $n = 0, 1, 2$ or 3 bosons (or n up and $3 - n$ down spins per triangle in the spin language). This leaves $3 - n$ bosons (or $3 - n$ up and n down spins) to be distributed over triangles which contain a C site of the dual lattice. Such a distribution must have the requisite periodicity of the wavefunction *i.e.* a 4×12 unit cell which involves 4 A sites (4 hexagons of the real lattice) in the x direction and 12 A sites (12 hexagons of the real lattice) in the y direction. Thus we find a multitude of energy-equivalent mean-field states with 4×12 units cells which corresponds to different ways of filling these sites keeping the total boson density (or magnetization) fixed to $3 - n$ on the C sites. Similar to the case of XXZ model on a Kagome lattice analyzed in Ref. 5, these states can superpose in the presence of quantum fluctuations leading to a pattern having n Bosons in every triangle which has a B site of the dual lattice at its center and $3 - n$ bosons

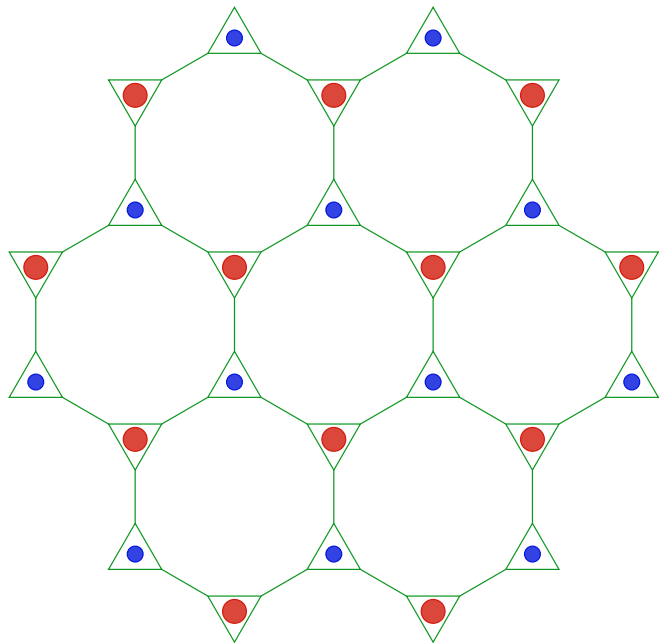


FIG. 18: Another possible state at $f = 1/2$ for $n = 2$. The large (red) circles indicate B sites and the corresponding triangles have one dimerized bond and an up spin while the small (blue) circles mean a triangle with one dimerized bond and a down spin. A similar state for $n = 1$ can occur and can be obtained by simply interchanging the sizes (colors) of the B and the C sites. This state is identical to the VBC-Néel phase predicted by QMC when quantum fluctuations are included. See text for details.

(on the average) in every triangles which has a C site of the dual lattice at its center. Now if we allow the spins on the joining links of these triangles to hybridize, we get a translationally invariant dimerized state, shown in Fig. 17, where each of the connecting bonds of the triangle can form a singlet dimer. This state is analogous to the VBC1 state obtained in QMC study. Another possible state, shown in Fig. 18 which correspond to $n = 2$ or $n = 1$, where the one bond in each of these triangles can hybridize (or form a valence bond), leads to the translation symmetry broken state shown in Fig. 18. This state is analogous to the VBC-Néel state found in QMC studies for $J^T \neq J^E$. There may be other possible states and a full classification of all of them seems to be difficult. We point out that the classification of these Mott states necessarily requires incorporation of quantum-fluctuation induced superposition between possible mean-field states.

IV. CONCLUSION

In conclusion, we have presented a study of Bose Hubbard or equivalently spin $1/2$ XXZ model on a star lattice using both QMC and dual vortex theory. We have shown that for $J^T = J^E$, the model supports translationally invariant RVB Mott phases at $f = 1/2$ and $f = 1/3$

and have pointed out that these phases are different from their counterparts with broken translational symmetry in square, triangular and Kagome lattices. We have also shown that these phases, upon increasing the ratio of nearest neighbor hopping amplitude to interaction strength, undergo a direct second order quantum phase transition to a superfluid phase. We have identified the exponents of this transitions and shown that they belong to the (2+1)D inverted XY universality class with $z = 1$ and $\nu = 2/3$ when approached through the tip of the Mott lobe. When the transition is approached from the side of the Mott lobe for $f = 1/3$, QMC finds a second order transition with $z = 2$. Such clear signatures of second order quantum phase transitions is in contrast with the behavior of the model on square, triangular or Kagome lattice, where these transitions are either first-order or

are accompanied by intermediate supersolid phases. We have also provided a phase diagram for the system at $1/2$ filling for $J^T \neq J^E$ and have demonstrated the existence of a Mott phase with coexisting density-wave (Néel) and RVB orders.

Acknowledgments

This work was supported by the Swiss National Science Foundation (SVI); the NSERC of Canada, the Canada Research Chair program, and the Canadian Institute for Advanced Research (YBK). Simulations were performed on the Brutus cluster at ETH Zürich.

-
- ¹ M. Greiner, O. Mandel, T. Esslinger, T. W. Hansch, and I. Bloch, *Nature (London)* **415**, 39 (2002).
² C. Orzel, A. K. Tuchman, M. L. Fenselau, M. Yasuda, and M. A. Kasevich, *Science* **291**, 2386 (2001).
³ L. Balents, L. Bartosch, A. Burkov, S. Sachdev, and K. Sengupta, *Phys. Rev. B* **71**, 144508 (2005); *ibid* **71**, 144509 (2005); L. Balents, L. Bartosch, A. Burkov, S. Sachdev, and K. Sengupta, *Prog. Theor. Phys. Suppl.* **160**, 314 (2005).
⁴ A. A. Burkov and L. Balents, *Phys. Rev. B* **72**, 134502 (2005).
⁵ K. Sengupta, S. V. Isakov, and Y. B. Kim, *Phys. Rev. B* **73**, 245103 (2006).
⁶ S. V. Isakov, S. Wessel, R. G. Melko, K. Sengupta, and Y. B. Kim, *Phys. Rev. Lett.* **97**, 147202 (2006).
⁷ M. Boninsegni, N. Prokof'ev, and B. Svitsunov, *Phys. Rev. Lett.* **96**, 070601 (2006); A. B. Kuklov, N. V. Prokof'ev, B. V. Svitsunov, M. Troyer, *Ann. Phys.* **321**, 1602 (2006).
⁸ S. Wessel and M. Troyer, *Phys. Rev. Lett.* **95**, 127205 (2005); D. Heidarian and K. Damle, *Phys. Rev. Lett.* **95**, 127206 (2005); R. G. Melko, A. Paramekanti, A. A. Burkov, A. Vishwanath, D. N. Sheng, and L. Balents, *Phys. Rev. Lett.* **95**, 127207 (2005).
⁹ S. Wessel, *Phys. Rev. B* **75**, 174301 (2007).
¹⁰ G. Misguich and P. Sindzingre, *J. Phys.: Condens. Matter* **19**, 145202 (2007).
¹¹ J. Richter, J. Schulenburg, A. Honecker, and D. Schmalz, *Phys. Rev. B* **70**, 174454 (2004).
¹² G. Misguich and C. Lhuillier, cond-mat/0310405 (unpublished).
¹³ T.-P. Choy and Y. B. Kim, arXiv:0903.3408 (unpublished).
¹⁴ K. Louis and C. Gros, *Phys. Rev. B* **70**, 100410(R) (2004).
¹⁵ A. W. Sandvik, *Phys. Rev. B* **59**, R14157 (1999); O. F. Syljuåsen and A. W. Sandvik, *Phys. Rev. E* **66**, 046701 (2002).
¹⁶ J. Vidal, R. Mosseri, and B. Douçot, *Phys. Rev. Lett.* **81**, 5888 (1998); J. Vidal, P. Butaud, B. Douçot, and R. Mosseri, *Phys. Rev. B* **64**, 155306 (2001).
¹⁷ C. Dasgupta and B. I. Halperin, *Phys. Rev. Lett.* **47**, 1556 (1981).
¹⁸ B. I. Halperin, T. C. Lubensky, and S.-k. Ma, *Phys. Rev. Lett.* **32**, 292 (1974).